JOURNAL OF GEOPHYSICAL RESEARCH, VOL. 101, NO. A12, PAGES 26,719–26,728, DECEMBER 1, 1996

High-latitude Hall and Pedersen conductances during substorm activity in the SUNDIAL-ATLAS campaign

M. Lester and J. A. Davies

Radio and Space Plasma Physics Group, Department of Physics and Astronomy
University of Leicester, Leicester, England

T. S. Virdi

Department of Physics, University College Wales, Aberystwyth, Dyfed, Wales

Abstract. Simultaneous high time resolution observations of the Hall and Pedersen conductances, Σ_H and Σ_P, respectively, the ionospheric electric field and the ground magnetic field during a magnetospheric substorm are reported. The measurements discussed here were taken during the SUNDIAL/ATLAS 1 campaign of March 24 to April 2, 1992. The European Incoherent Scatter (EISCAT) UHF special programme SP-UK-ATLAS, which operated on March 27, 1992, provided continuous measurements of the electron density and the ion vector velocity from which Σ_H and Σ_P and the ionospheric electric field were calculated. During the substorm growth phase, Σ_P and Σ_H were less than 10 S and the ratio, $R = \Sigma_H / \Sigma_P$, was less than 1. Although both Σ_H and Σ_P increased at the onset of the expansion phase, R remained close to 1. This ratio provides information on the mean energy of the precipitating particles responsible for the enhanced conductances. A ratio of 1 implies a mean energy of the particles of 2.56 keV. Two distinct expansion phases were identified, the second of which included a number of intensifications. Both Σ_H and Σ_P increased toward the end of the second expansion phase with peak values of 71 S and 34 S, respectively. The ratio R also increased to values exceeding 2, equivalent to mean energies of more than 5.78 keV. The largest value of R was 3.25, which occurred during the substorm recovery phase and is equivalent to mean energies of more than 10 keV. The increase in mean energy as the substorm progresses may be interpreted in terms of changes in the acceleration processes in the magnetosphere. The maximum zonal (east-west) current during this interval was 2.20 A m^{-1} and occurred toward the end of the second substorm expansion phase. At a number of intensifications, reversals or enhancements in the zonal current were observed, for which the electric field was responsible in most cases. While the peak value of the Pedersen conductance of 40 S is similar to recent published results, the Hall conductance peak of 75 S is less than recent published measurements. Furthermore, the westward current during the initial part of the expansion phase is dominated by the electric field, in contrast to a previously published model which suggested that this current would be conductivity dominated. It is suggested that further spatial structure of the current is necessary to explain these observations.

1. Introduction

Modeling the large-scale three-dimensional current systems associated with the coupling of the ionosphere and magnetosphere has developed considerably in recent years [e.g., *Richmond and Kamide*, 1988; *Emery et al.*, 1990; *Lu et al.*, this issue]. In particular, the technique of assimilative mapping of ionospheric electrodynamics (AMIE) can be employed to derive the distribution of the ionospheric conductances, electric fields, currents, and other related quantities at high latitudes. Inputs to the model include radar and spacecraft measurements of electric fields or plasma velocities. The main input to the model, however, is magnetometer data, and the results are dependent upon the ionospheric conductance. Usually, models of conductance [e.g., *Spiro et al.*, 1982; *Fuller-Rowell and Evans*, 1987] are employed in this technique, although radar and satellite estimates of conductance can be included [e.g., *Knipp et al.*, 1989]. The height-integrated Pedersen and Hall conductivities, the Pedersen and Hall conductances, can be inferred from spacecraft measurements of precipitating electrons [e.g., *Spiro et al.*, 1982; *Fuller-Rowell and Evans*, 1987]. Incoherent scatter radar measurements of plasma density can also provide estimates of Pedersen and Hall conductances, Σ_P and Σ_H respectively [e.g., *Brekke et al.*, 1974, 1989; *Kirkwood et al.*, 1988]. Spacecraft measurements can be made over a large spatial scale but cannot provide information of the temporal evolution of the measurements. Conversely, the ground-based incoherent scatter measurements have a limited spatial coverage but the temporal coverage is excellent. The AMIE modeling provides a global coverage with improved temporal resolution but is reliant on data inputs.

Perturbations of the ground magnetic field can arise due to enhancements in conductivity, enhancements in electric field, or some combination of both. The high-latitude nightside region is particularly susceptible to large-scale magnetic perturbations,

Paper number 96JA00979.
0148-0227/96/96JA-00979$09.00

especially during magnetospheric substorms. The large-scale auroral disturbances during substorms as well as potentially large electric fields associated with the destruction of open magnetic flux in the magnetotail can result in excursions of the horizontal and vertical magnetic field which can be greater than 500 nT. For the purposes of modeling the ionospheric electrodynamics in this region it is necessary to have a complete picture of the behavior of the conductivity and electric field. Unfortunately, there have been relatively few attempts to undertake simultaneous measurements of the ionospheric electric field and conductivity during substorms. The Chatanika incoherent scatter radar provided the first results of such simultaneous measurements (see, for example, *Kamide and Vickrey* [1983, and references therein]). *Kamide and Vickrey* [1983] concluded that in the eastward electrojet in the evening sector, the magnitude of the northward electric field increased when the magnitude of the electrojet increased. Furthermore, Σ_H remained at ~ 10 S even when the current density became as large as 1 A m^{-1}. The westward electrojet, however, appeared to have two separate components. In the 0000 - 0300 MLT sector, the electrojet intensity was maintained by a weak southward electric field and a high Σ_H. After 0300 MLT, however, the electrojet was dominated by a strong southward electric field.

While these results provide an important insight into the behavior of Σ_H and electric fields, *Kamide and Vickrey* [1983] pointed out a number of caveats that needed to be considered because of limitations with the experiment. One of these was the large uncertainties in the north-south electric field measurements. It has become apparent from tristatic measurements of ion velocity by EISCAT that the *F* region electric field perpendicular to the magnetic field can vary on short (~1 min) timescales [*Williams et al.,* 1990, 1992]. It is important therefore that simultaneous measurements of electric field and conductance be made to confirm the earlier results of *Kamide and Vickrey* [1983]. EISCAT is well suited to the task of making simultaneous high time resolution measurements of the Hall and Pedersen conductances and electric fields, especially during the various phases of substorm activity.

Such an EISCAT study, employing high time resolution measurements along the magnetic field of Σ_H and Σ_P, in conjunction with electric field measurements made at 300 km on the same field line, was reported by *Kirkwood et al.* [1988]. Unfortunately, the EISCAT experiment utilized in this study did not make continuous measurements of the *F* region electric field. *Kirkwood et al.* [1988] did, however, utilize auroral images from the Viking spacecraft in order to place the observations of Σ_H, Σ_P, and the electric field in a spatial context as well as in relation to substorm phases. Concentrating on conductances associated with the substorm westward electrojet, *Kirkwood et al.* [1988] found that Σ_H varied between 15 S and 30 S and the ratio *R* of Σ_H and Σ_P between 2 and 2.5, with little variation from one substorm to another. These observations were made within the diffuse aurora. Conductances in the discrete aurora leading the westward traveling surge (WTS) and the auroral bulge were much higher. In these locations Σ_H varied between 60 S and 100 S and *R* between 2 and 4. The highest observed values of Σ_H and Σ_P were 120 S and 48 S, respectively, at the equatorward edge of the WTS. More recently, a similar study by *Aikio and Kaila* [1996], who were able to use continuous simultaneous measurements of Σ_H, Σ_P and the electric field, illustrated that Σ_H could be as high as 214 S near the poleward boundary of the auroral bulge during the substorm expansion phase. At the same time, Σ_P remained less than 40 S. The ratio of the two conductances, *R*, was as high as 5.2 at this location. During the growth phase, large values of both conductances, up to 30 S, were reached when discrete auroral forms passed through the radar beam.

Previous estimates of conductances during substorms had also been made by modeling ground magnetometer data and STARE estimates of the electric fields. During auroral breakups at the substorm expansion phase onset, *Baumjohann et al.* [1981] estimated peak values of 30 S for Σ_H and 10 S for Σ_P close to the western edge of the auroral active region. In the higher conducting region behind the head of the WTS, *Opgenoorth et al.* [1983] suggested values of 25 S and 20 S for the Hall and Pedersen conductances, respectively.

The first ATLAS mission [*Torr*, 1993] of March 24, 1992 to April 2, 1992, was the focus for a coordinated ground-based campaign involving the SUNDIAL experimenters [*Szuscsewicz et al.,* this issue]. As part of this ground-based campaign, the European Incoherent Scatter (EISCAT) UHF radar was operated for a short, 6-hour, interval on March 27, 1992 in a special mode, SP-UK-ATLAS. An extended CP-1-J run of the EISCAT UHF radar also took place during the latter part of the ATLAS mission. This paper presents estimates of Σ_P and Σ_H and associated electric fields during substorm activity from the interval on March 27, 1992.

2. Overview of 1800 - 2200 UT, March 27, 1992

The run of the EISCAT UHF special programme SP-UK-ATLAS took place between 1600 and 2200 UT on March 27, 1992. This experiment was effectively the CP-1-J experiment (see, for example, *Davies et al.* [1995]) in which the Tromsø beam is pointed parallel to the magnetic field at an altitude near the *F* region peak. The one significant difference, however, in the SP-UK-ATLAS experiment is the continuous intersection of the beams from the two remote site antennas, at Sodankylä and Kiruna, with the Tromsø beam at a fixed height of 275 km. In CP-1-J, the remote sites intersect the Tromsø beam at 278 km for only 90 s in every 5 min, with the remaining time being spent in the *E* region. In both the CP-1-J and SP-UK-ATLAS experiments the same pulse schemes are transmitted, long pulse for observations between 150 and 550 km, two power profiles and an alternating code for measurements between 80 and 270 km. The SP-UK-ATLAS experiment provides continuous high time resolution estimates of the electric field in the *F* region which therefore allows us to make simultaneous high time resolution measurements of conductance and electric fields. We concentrate on the interval 1800 - 2200 UT and summarize the EISCAT observations below.

The *F* region electron density and electron temperature were highly variable between 1800 and 2200 UT. The peak value of electron density in the *F* region varied between 5 x 10^{11} m^{-3} and 9 x 10^{11} m^{-3} and the altitude of the peak varied between about 250 and 450 km, generally increasing toward the end of the interval. The electron temperature was enhanced between 1830 and 1900 UT and after 1930 UT shorter-lived periods of enhanced electron temperature were observed. Several short intervals of enhanced ion temperature resulting from ion frictional heating [e.g., *McCrea et al.,* 1991] were also observed. At 1800 UT the ion velocity perpendicular to the magnetic field was westward and southward, becoming eastward from about 1900 until 1930 UT. Variable flow followed with values reaching 1 km s^{-1}. After 2015 UT the ion velocity remained eastward, apart from two 2-min intervals starting at 2044 and 2141 UT.

The alternating code measurements illustrating enhanced levels of E region ionisation provide evidence that particle precipitation occurred over much of the interval. Between 1830 and 1900 UT there were strong levels of particle precipitation with values of electron density of order 1 x 10^{12} cm^{-3} at 120 km altitude, densities which are higher than the F region peak densities observed in the interval. The precipitation, however, did not penetrate to altitudes much lower than 118 km. After 1930 UT there were several bursts of precipitation again only penetrating to about 118 km. After about 2040 UT, stronger and more continuous precipitation occurred and penetrated to about 100 km.

In summary, the SP-UK-ATLAS observations between 1800 and 2200 UT on March 27, 1992, can be divided into four separate periods: 1800 - 1823 UT when there is no electron or ion heating and the ion velocity is westward with a magnitude less than 400 m s^{-1}; 1823 - 1855 UT when there were intervals of precipitation into the E and F regions, continuous electron heating prefaced by a short-lived ion heating event corresponding to a high ion velocity peaking at 1827 UT; 1855 - 1935 UT during which there was precipitation but only into the F region and some intervals of electron and ion heating with variable westward/eastward ion velocity; 1935 - 2200 UT when there was precipitation initially to 118 km and then to 100 km, variable flow initially and then eastward flow between 400 and 800 m s^{-1} from 2015 UT.

The IMAGE network [*Lühr*, 1994], which is based upon the EISCAT magnetometer cross [*Lühr et al.*, 1984], can provide information on the auroral electrojet currents flowing in the vicinity of EISCAT during the interval. The locations of the specific stations from the IMAGE array which have been used in this study are given as stars in Figure 1. The location of the EISCAT beam during the SP-UK-ATLAS experiment at 120 km altitude is represented by a square. Investigation of magnetometer data from the IMAGE network demonstrates that

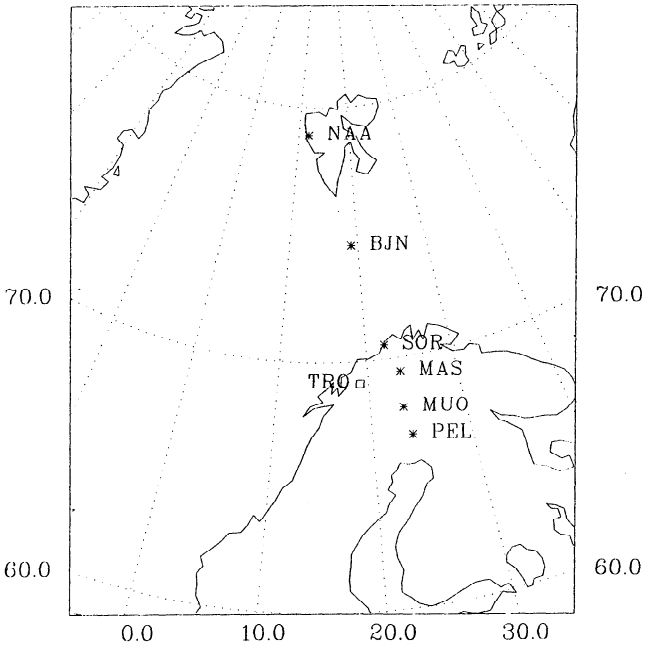

Figure 1. A map showing the locations of the IMAGE magnetometer stations used in this study and the position of the EISCAT beam at an altitude of 120 km during the experiment.

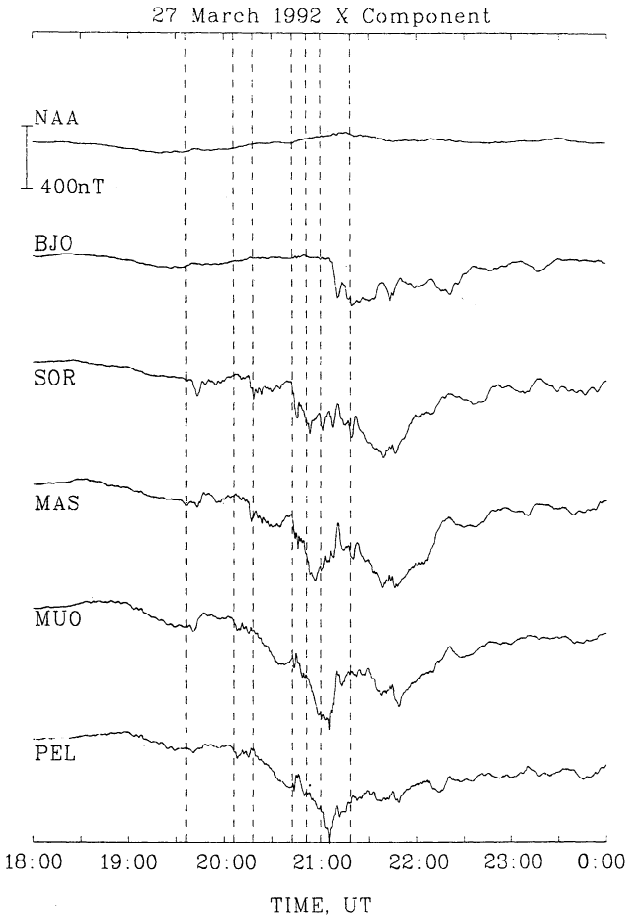

Figure 2. The X (north-south) component of the magnetic field measured at selected stations from the IMAGE magnetometer array for the interval 1800 - 2400 UT on March 27, 1992. The dashed vertical lines represent the times of Pi 2 Pulsations identified in the SAMNET data (not shown).

the interval 1800 - 2200 UT contains substorm activity (Figure 2). One sensitive indicator of the substorm expansion phase and subsequent intensifications is the Pi 2 pulsation [*Rostoker et al.*, 1980] and the first Pi 2 identified in the SAMNET data [*Yeoman et al.*, 1990] was at 1936 UT. This was followed by Pi 2 pulsations at 2006, 2018, 2042, 2051, 2100, and 2118 UT, where all times are accurate to within 1 min. These times are identified in Figure 2 by the vertical lines. The first of these was associated with a weak negative X (north-south) component bay at SOR of approximately 100 nT, which is indicative of a weak westward electrojet. Negative excursions of the X component were associated with subsequent Pi 2 pulsations at 2006 UT (MUO and PEL), 2018 UT (SOR and MAS), 2042 UT (SOR and MAS), 2051 (MAS and MUO), and 2100 UT (PEL). The magnitudes of the bays associated with the pulsations were low to start (~-100 nT), but larger at the times of the later pulsations (-200 to -300 nT). The integral effect was negative bays of up to -800 nT at MUO and -500 nT at SOR compared with the quiet time magnetic variation. After the last Pi 2 pulsation, there was a general recovery of the magnetic field at all of the stations, although the minimum value of the X component occurred at different times at different stations. Further discussion of the electrojets and substorm current wedge associated with the substorm intensifications will follow in section 4.

Substorm identification can be difficult and often a single characteristic phenomenon may not be sufficient to identify all substorm expansion phases and intensifications [*Yeoman et al.*, 1994]. Another often used indicator of magnetospheric substorms is the particle injection at geosynchronous orbit [e.g., *Lanzerotti et al.*, 1971; *Belian et al.*, 1981]. Such particle injections can either be dispersionless in energy, which generally indicates that the spacecraft is close to the field lines which map to the auroral breakup region, or dispersed in energy which indicates that the particles, once injected into the near-Earth tail, have undergone curvature and gradient drift [*Reeves et al.*, 1991]. Electron fluxes in the 30 - 500 keV range from four geosynchronous spacecraft operated by Los Alamos indicate only one large-scale dispersionless injection, at 2009 UT at spacecraft 1991-030 which was located at a local time of ~0051 MLT. This was followed by a series of four increases in the particle flux at the same spacecraft at 2018, 2030, 2045, and 2106 UT which were also all dispersionless and are indicative of subsequent substorm intensifications. There followed, at the three other spacecraft, dispersed injections where the flux of the higher-energy particles peaked before that of the lower-energy particles. These dispersed injections could in general be related to the dispersionless injections observed by spacecraft 1991-030. One event, at 1848 UT, was observed by spacecraft 1989-046 at a time of 0746 MLT and could not be related to a dispersionless injection at any of the four spacecraft or to any other evidence of

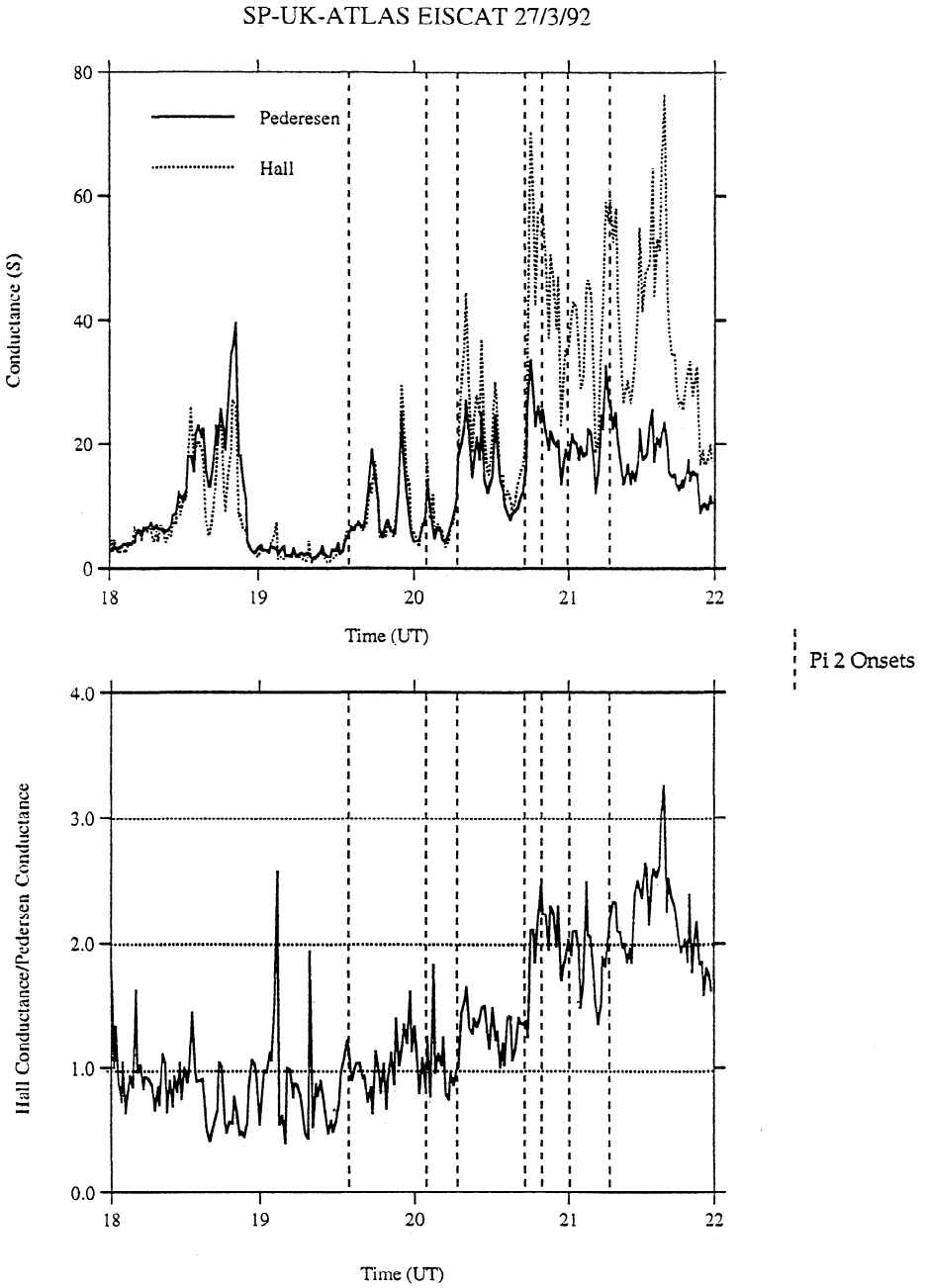

Figure 3. (top) The Pedersen (solid line) and Hall (dotted line) conductances are plotted as a function of universal time from 1800 to 2200 UT. (bottom) The ratio of Hall to Pedersen conductance for the same interval. The dashed vertical lines in each panel represent the times of the Pi 2 pulsations.

substorm activity, although particle precipitation into the E region was indicated by EISCAT observations between 1823 and 1855 UT.

In summary, separate substorm expansion phases occurred at 1936 and 2006 UT. An earlier expansion phase may have occurred before 1848 UT although this is difficult to confirm. The expansion phase at 2006 UT involved a Pi 2 pulsation, an enhanced westward electrojet and particle injection in the near-Earth tail and was followed by a number of intensifications. We argue that this is a separate expansion phase from the one at 1936 UT on the basis of the time difference from the first event of more than 20 min, a similar time difference to that employed by *Farrugia et al.* [1993] in their study of substorm activity during the passage of an interplanetary magnetic cloud. This second expansion phase lasted until at least 2118 UT, the time of the final Pi 2 pulsation. During each expansion phase there were intervals of particle precipitation into the lower ionosphere which modified the Pedersen and Hall conductivities. No solar wind plasma or IMF measurements are available for this interval.

3. Hall and Pedersen Conductances

The Hall and Pedersen conductances, Σ_H and Σ_P, respectively (Figure 3) have been calculated between 1800 to 2200 UT from the EISCAT SP-UK-ATLAS alternating code measurements of electron density, analysed at an integration time of 60 s. The conductances were calculated over the altitude range 86 - 200 km along the magnetic field direction. The ion-neutral and electron-neutral collision frequencies were calculated using the MSIS-86 model [*Hedin,* 1987] to provide estimates of the neutral atmospheric composition and temperature within the altitude range of interest. Estimates of the ion and electron gyrofrequencies were based on values of the magnetic field from the IGRF model. The magnetic latitude of Tromsø is between that of SOR and MAS, but its longitude is some 5° to the west of these stations.

The conductances were typically a few siemens at the start of the interval (Figure 3, top). Between 1828 and 1855 UT, both Hall (dotted line) and Pedersen (solid line) conductances increased above 10 S, reaching peak values for Σ_P of 40 S at 1851 UT and 27 S at 1850 UT in the case of Σ_H. The ratio of the two conductances, $R = \Sigma_H/\Sigma_P$, (Figure 3, bottom) remained, in general, less than one. Following 1855 UT, both Σ_P and Σ_H decreased to below 10 S and remained so until about 2015 UT apart from three brief intervals centred at 1944, 1956, and 2005 UT. Between 1855 and 2015 UT the ratio of the two conductances remained close to 1. Both Σ_P and Σ_H were higher following 2016 UT, with the former peaking at values of between 22 and 27 S and the latter peaking at values between 30 and 45 S. Higher conductances continued until 2036 UT, during which time R was between 1 and 1.5. After 2036 UT, Σ_P and Σ_H increased again, with Σ_P peaking at values between 20 and 33 S, while Σ_H now peaked at values above 50 S, and was well above 20 S until 2153 UT. Between 2016 and 2100 UT the ratio of the two conductances was typically between 1.5 and 3.

The variation of R as a function of time (Figure 3, bottom) demonstrates that the interval can be divided into two parts. The first from 1800 to 2000 UT, where R was typically of order 1, and the second from 2000 to 2200 UT where R was typically larger than 1 and often of order 2 or more. The zonal component of the ion velocity was typically eastward during the first interval and westward during the second. Figure 4 further demonstrates the relationship between Σ_H and Σ_P for the two parts of the

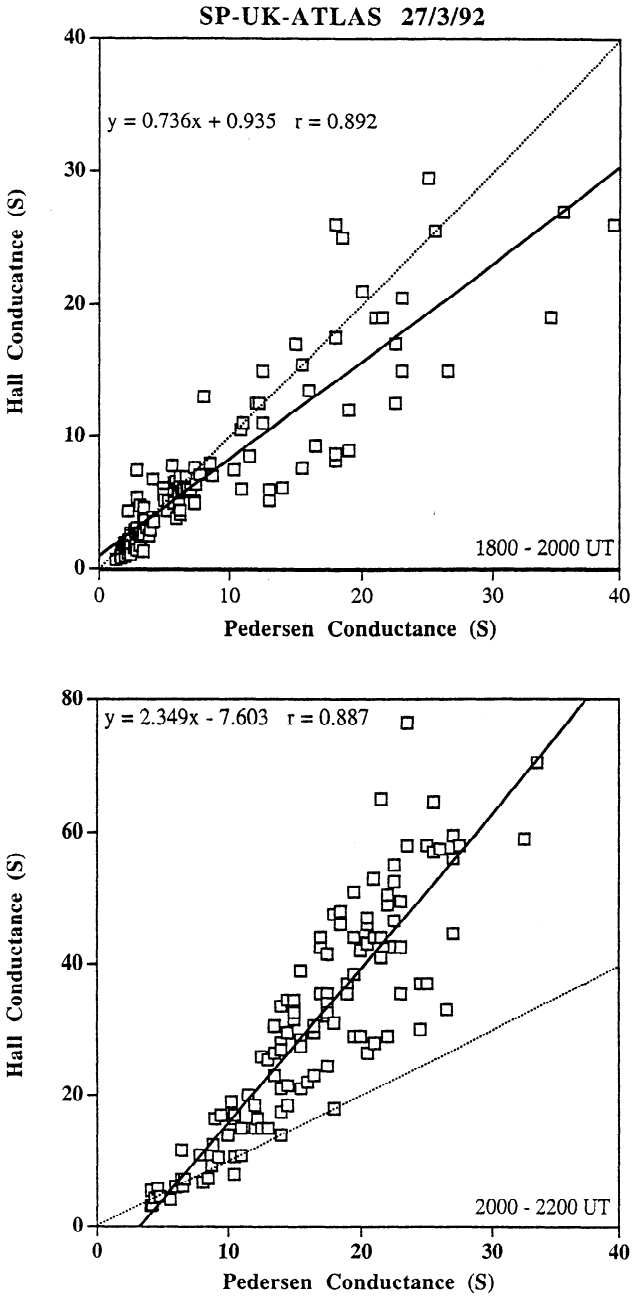

Figure 4. (top) The Hall conductance is plotted as a function of the Pedersen conductance for the interval 1800 - 2000 UT. The dashed line represents Hall conductance equaling Pedersen conductance. The solid line represents the best fit linear function with the relationship at the top of the panel together with the correlation coefficient. (bottom) The same but for the interval 2000 - 2200 UT. Note the difference in scale for the Hall conductance in this panel.

interval. Between 1800 and 2000 UT (Figure 4, top), the two conductances were similar, although Σ_P was typically larger than Σ_H, with most values below 10S. Between 2000 and 2200 UT (Figure 4, bottom) Σ_H had a much wider distribution of values and was closer to twice the value of Σ_P. *Robinson et al.* [1987] have demonstrated that the ratio R is given by

$$R = 0.45\,E^{0.85}$$

where E is the average energy in keV of the precipitating electrons. From this expression we note that a ratio of 1 is

produced by precipitating electrons with average energy of 2.56 keV, while to produce a ratio of 2, the average energy of the precipitating electrons would be 5.78 keV. These values illustrate that the average energy of the particle spectrum during the second interval was higher with more particles penetrating to lower altitudes. Thus not only did the level of precipitation increase but also the particle spectrum changed from the first to the second interval. Discussion of the conductances and their relationship to substorm phase is given in section 4.

The electric field measurements by EISCAT were made at a height of 275 km, compared with the conductances which were measured between 86 and 200 km. Although the EISCAT beam was parallel to the magnetic field at 275 km, the nature of the magnetic field is such that the measurements at lower altitudes were not exactly on the same field line. The differences are, however, small and we assume that measurements of electric field, Σ_P, and Σ_H are effectively along the same field line. Before discussing in detail the electric field variation we note that the integration period of 1 min is not short enough to cope with extremely short lived (a few seconds) variations in the electric field recently measured by EISCAT [*Lanchester et al.*, 1996]. For the purposes of this study, however, a temporal resolution of 1 min is more than adequate.

The components of the electric field perpendicular to the magnetic field are illustrated in Figure 5. The north-south component (positive north) is typically larger than the east-west component (positive east), although the latter is between -10 mV m^{-1} and -25 mV m^{-1} for much of the interval. At 1800 UT the electric field is directed northward and westward and around 1900 UT both components change direction, consistent with the motion of the radar through the electric field Harang Discontinuity. Following the first expansion phase onset at 1936 UT, the north-south component returns northward. It is only following the Pi 2 pulsation at 2018 UT, however, that the field remains consistently southward, apart from two very brief intervals. The magnitude of the north-south component during this interval is typically larger than 25 mV m^{-1}. All but the last of the Pi 2 pulsations are followed by an enhancement or a change in direction of the north-south electric field. Only the events at 2018 and 2042 UT had simultaneous increases in Σ_H.

4. Discussion

It is instructive to consider how the conductances varied as a function of substorm phase. The interval has been divided into a growth phase, two expansion phases, the second of which is divided into three separate intervals, and a recovery phase. Average values of Σ_H, Σ_P and R plus their ranges are given in Table 1 for each of these intervals. As there were no interplanetary magnetic field (IMF) data, it is not possible to identify the time of any southward turning which is normally expected to be the initiation of the substorm growth phase [*Lester et al.*, 1993]. Since the growth phase is generally expected to last between 30 and 60 min [*Lui*, 1991], we have selected the interval 1900 - 1935 UT as representative of the growth phase in this case. Taking a longer interval may have included the response to the possible expansion phase identified by the geosynchronous spacecraft 1989-046, which observed an energy dispersed particle injection at 1848 UT. During the growth phase, Σ_H and Σ_P were both typically less than 3 S and their ratio R less than 1.0. The average values of Σ_H and Σ_P between 1900 and 1935 UT were 2.4 S and 2.7 S respectively and the mean value of R was 0.88 (see Table 1).

The interval following the first Pi 2 pulsation, 1936 to 2005 UT, is taken to represent the first expansion phase. There was a clear increase in both Σ_H and Σ_P, to 9.3 S and 9.6 S respectively, in the expansion phase, although R was only marginally larger than in the growth phase. The second expansion phase, which followed the first of the dispersionless injections, is divided into three intervals, 2006 - 2018 UT, 2018 - 2042 UT, and 2042 -

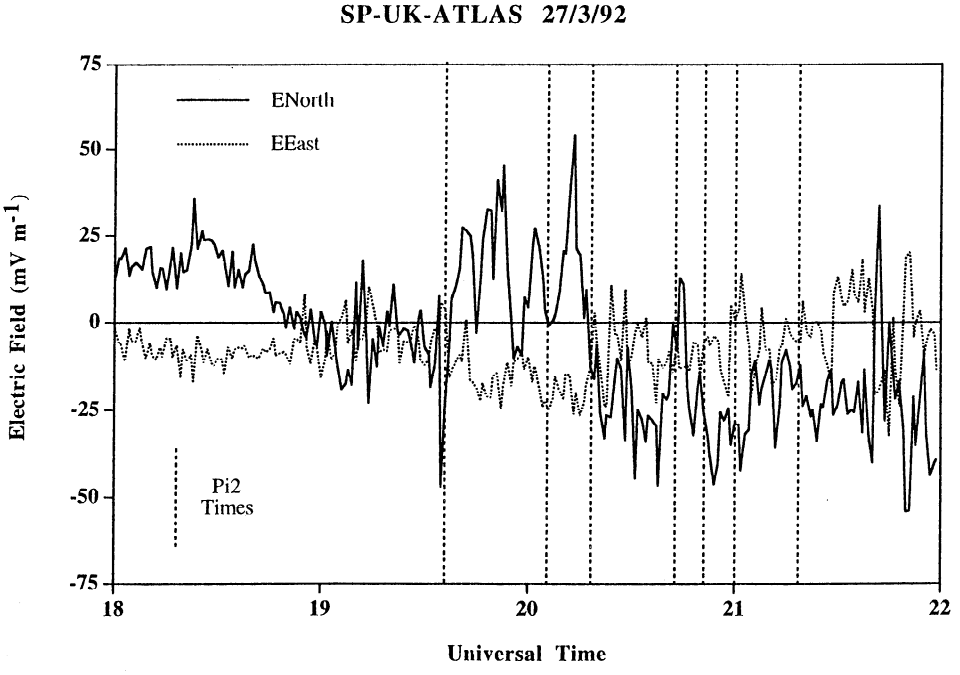

Figure 5. The north-south (solid line) and east-west (dotted line) components of the electric field measured by EISCAT is plotted for the interval 1800 - 2200 UT. The dashed vertical lines in each panel represent the times of the Pi 2 pulsations.

Table 1. Summary of the Hall and Pedersen Conductances and the Ratio R for the various phases of the substorm.

Interval	Mean			Range		
UT	Σ_H (S)	Σ_P (S)	R	Σ_H (S)	Σ_P(S)	R
Growth						
1900 - 1935	2.4	2.7	0.88	0.7 - 7.5	1.3 - 5.0	0.38 - 2.57
Expansion 1						
1936 - 2006	9.6	9.3	1.02	3.4 - 29.5	4.2 - 25.0	0.63 - 1.61
Expansion 2						
2006 - 2018	7.8	7.7	1.02	3.2 - 18.0	4.1 - 18.0	0.74 - 1.82
2018 - 2042	21.1	15.6	1.32	9.3 - 44.5	7.9 - 27.0	1.00 - 1.65
2042 - 2130	40.6	20.2	1.99	16.5 - 70.5	12.0 - 33.5	1.25 - 2.50
Recovery						
2130 - 2200	36.3	15.8	2.22	16.5 - 76.5	9.0 - 25.5	2.59 - 3.25

2130 UT. The first two of these intervals begin with a Pi 2 pulsation and include no other pulsation activity. The third interval includes the last three Pi 2 pulsations (or substorm intensifications). During the first of these intervals (2006 - 2018 UT), Σ_P, Σ_H, and R were similar to the earlier expansion phase. During the second (2018 - 2042 UT), however, there was a significant increase in all three parameters with three major peaks, at 2020 UT (Σ_H was 45 S and Σ_P 22 S), at 2026 UT (Σ_H was 37 S and Σ_P 25 S), and 2031 UT (Σ_H was 30 S and Σ_P 25 S). In the third interval (2042 - 2130 UT), all three parameters again increased. Σ_H and Σ_P peaked at 71 S and 34 S, respectively, at 2045 UT after which both then tended to decline with Σ_H showing the highest variability.

The recovery phase of the substorm followed the last of the Pi 2 pulsations. The onset of the recovery phase is difficult to identify as the minimum values of the negative bays in the IMAGE stations occurred at very different times. We have, therefore, chosen the interval 2130 to 2200 UT (the end of the data) as representative of the initial part of the recovery phase if not the full recovery phase. During the first ten minutes of the recovery phase, Σ_H was larger than 40 S with peaks of 65 and 77 S at 2134 and 2139 UT, respectively. Following this last peak, Σ_H decreased in an almost monotonic fashion to 20 S at 2200 UT. The corresponding peaks in Σ_P were 26 and 24 S, and Σ_P decreased to 10 S at 2200 UT. The ratio R was larger than 2 until 2145 UT, with a peak value of 3.25 at 2139 UT. During the last 15 min, R was between 1.6 and 2.4. The mean value of Σ_H was 36.3 S, Σ_P was 15.8 and R was 2.22 (see Table 1).

In summary, we find that the Pedersen conductance was dominant during the growth phase, the first expansion phase and the initial part of the second expansion phase. The Hall conductance eventually became dominant in the latter part of the expansion phase and continued to dominate well into the recovery phase. Indeed, the ratio R was largest in the earliest stages of the recovery phase. The largest value of Σ_P was 34 S which occurred late in the expansion phase, although a higher value had occurred as part of the possible expansion phase before 1848 UT. The largest value of Σ_H of 76 S occurred in the early recovery phase. The increase in R from less than 1, in the growth phase, to greater than 3 in the recovery phase, demonstrated an increase in the average energy of the electrons which resulted in the enhanced conductances.

Before comparing these observations with previous results, it is helpful to determine the location of the substorm currents relative to Tromsø. The substorm current wedge [*McPherron et al.*, 1973] provides a simple representation of the large-scale currents associated with substorm expansion phase onset. At the time of the first Pi 2 pulsation, at 1936 UT, the current wedge was located east of the SAMNET array and hence east of Tromsø. The X component at SOR was indicative of a westward electrojet whereas at Tromsø the direction of the ion velocity in the F region became westward immediately after the Pi 2 pulsation. The zonal (east-west) current derived from the observations by EISCAT (Figure 6) was initially westward at the onset of the Pi 2, but became eastward at 1939 UT and thereafter oscillated between westward and eastward until 2000 UT. For the next three Pi 2 pulsations, at 2006 UT, 2018 UT and 2042 UT, the centre of the current wedge was east of NUR (~102° magnetic longitude), whereas the western (upward) field-aligned current (FAC) was between GML and NUR (78 - 102° magnetic longitude). Unfortunately, the station at KVI (96° magnetic longitude) was not operational, and we are therefore unable to determine the position more accurately. The IMAGE array indicates a westward electrojet centred at latitudes equatorward of Tromsø. Following the first Pi 2 pulsation of this expansion phase at 2006 UT, there was a rapid increase in westward flow to values exceeding 1 km s^{-1}, at 2013 UT, but the ion flow had then turned eastward by 2015 UT. The current was eastward from 2001 to 2004 UT and then again from 2011 to 2014 UT. The peak in ion flow at 2013 UT also corresponded to a peak in current of ~76 mA m^{-1}, but following the pulsation at 2018 UT the westward current peaked at nearly 1 A m^{-1} at 2021 UT. Following the intensification at 2042 UT the zonal current measured by EISCAT briefly turned eastward. Thus Tromsø is likely to have been located poleward of the electrojet centre and possibly close to the downward FAC for the second expansion phase onset, at 2006 UT, east of this FAC for the following intensification at 2018 UT, and possibly back close to the FAC at 2042 UT. For the last three intensifications, at 2051 UT, 2100 UT and 2118 UT, the western FAC was west of GML (78° magnetic longitude), while the electrojet remained centred equatorward of Tromsø. The ion flow was eastward and the current was directed westward. Thus we expect Tromsø to have been located within the substorm current wedge during these intensifications.

We begin our comparison with previous estimates of conductances by considering the growth phase values. *Kirkwood et al.* [1988] noted that in the diffuse aurora associated with the

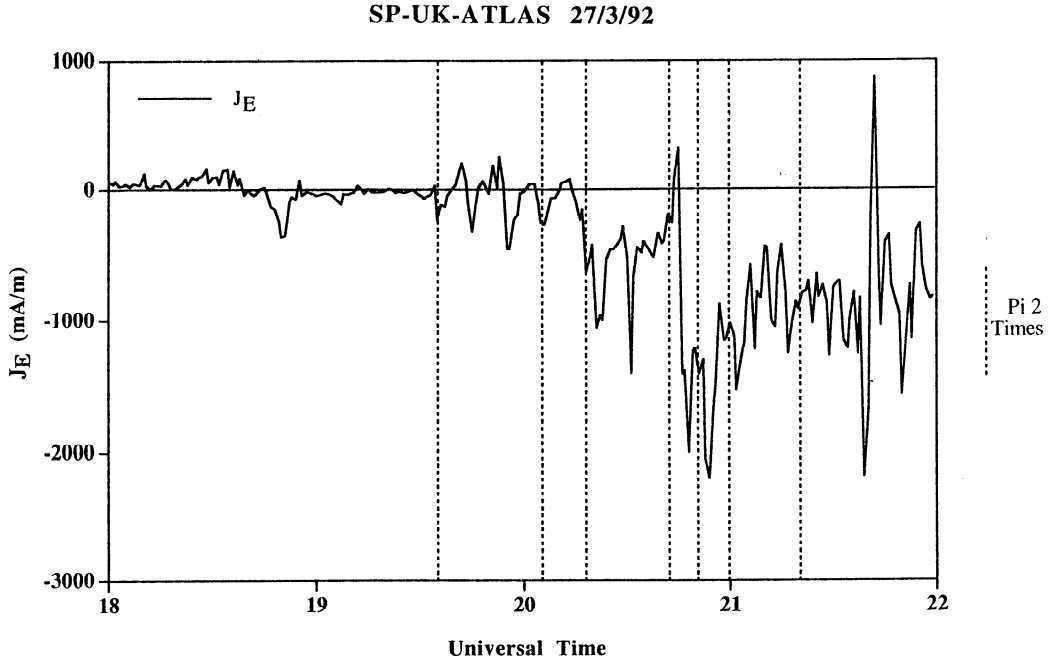

Figure 6 . The east-west current density for the interval 1800 - 2200 UT. The dashed vertical lines in each panel represent the times of the Pi 2 pulsations.

growth phase, Σ_H was typically between 2 and 15 S, Σ_P between 1 and 8 S, and their ratio R was between 1.6 and 2.0. The growth phase discussed above had values which were typically less than these; in particular, Σ_H reached a value of only 7.5 S, and the ratio R was typically less than 1. *Aikio and Kaila* [1996] report observations of Σ_H and Σ_P up to 30 S with EISCAT in conjunction with all-sky camaera optical measurements in the growth phase of a substorm in January 1993. These high values in the growth phase were measured in discrete auroral arcs. Outside of the arcs, Σ_H and Σ_P were typically between 2 and 3 S. Unlike *Kirkwood et al.* [1988] or *Aikio and Kaila* [1996], however, we have no direct evidence for the diffuse aurora in the radar beam during the growth phase. The values of Σ_H and Σ_P during the growth phase are higher than those measured in quiet periods during the extended run of CP-1 later in the campaign. We therefore believe that the values of Σ_H and Σ_P discussed here are related to particle precipitation associated with diffuse aurora. Other estimates of the growth phase conductances include 9 S for Σ_H [*Mishin et al.,* 1986], based upon a modified model of *Spiro et al.* [1982]. Assuming that the higher values of Σ_H and Σ_P during the growth phase are associated with particle precipitation, we can estimate the average energies of the precipitating electrons [*Robinson et al.,* 1987]. Assuming a Maxwellian electron distribution, the mean particle energy for values of R between 0.5 and 1 is typically between 1.13 and 2.56 keV [*Robinson et al.,* 1987].

The peak values of Σ_H and Σ_P during the first expansion phase, 29.5 and 25.0 S respectively, may have been associated with discrete auroral forms but the values of Σ_H are lower than those reported by *Kirkwood et al.* [1988] for discrete auroral forms at expansion phase onset, which were typically larger than 30 S. Furthermore, *Aikio and Kaila* [1996] report observations of Σ_P and Σ_H which reach 40 and 214 S, respectively, with a corresponding value for R of 5.4 at the poleward boundary of the auroral bulge. It is only during the later intensifications of the second expansion phase that Σ_H began to reach values similar to those associated with discrete arcs as well as expansion phase diffuse aurora of 15 - 30 S reported by *Kirkwood et al.* [1988] and *Aikio and Kaila* [1996]. Furthermore, we appear to have lower values of R, which may be due, in part, to the larger range of altitudes over which we have integrated the conductivity since there is a significant contribution to Σ_P at altitudes between 160 and 200 km. A comparison of Σ_P over the altitude range 86 - 200 km with Σ_P over the range 86 - 150 km, similar to that employed by *Kirkwood et al.* [1988] indicates the former is, on average over the whole interval, 20% higher than the latter. This does not fully account for the lower values of R reported here. We believe it is necessary to integrate up to altitudes of 200 km in order to gain a complete picture of the behavior of Σ_P. The location of the breakup region was, based upon the current wedge identification, close to Tromsø for the second expansion phase onset, 2006 UT, and again for the intensification at 2042 UT. At the times of other intensifications during the second expansion phase, Tromsø was to the east of the breakup region and within the westward electrojet. Values of R up to 2.5 indicate average particle energies of 7.52 keV associated with these conductances.

Both Σ_H and Σ_P reach high values, 76.5 and 25.5 S respectively, in the recovery phase. Neither *Kirkwood et al.* [1988] nor *Aikio and Kaila* [1996] discuss observations of conductances during the recovery phase. While there is considerable variability in the conductances during the recovery phase, the average values and the ranges are typically higher than at any other time in the substorm interval. It is unclear whether these values of conductance are associated with discrete or diffuse aurora. The recovery phase also includes the peak value of R of 3.3 which is consistent with mean energies of 10.42 keV. This suggests that the spectrum of the precipitating particles changed considerably by the time of the recovery phase. This could be due to acceleration processes in the tail which result in the increased average energy of the precipitating particles. If this

is so, then it suggests that the late expansion phase/early recovery phase is an important time within the substorm cycle in the tail. An alternative suggestion is that this is a spatial effect rather than a temporal one and that the radar has rotated into the region where the higher energy electrons are located. Such a study reported here cannot distinguish between the two possibilities. It is necessary, however, for future studies to investigate this in more detail.

It is instructive to calculate the current measured by EISCAT during the substorm interval. Rather than compute the Hall current we follow *Aikio and Kaila* [1996] who have computed the total current measured by EISCAT and in Figure 6 present the east-west component of this current. The peak value of the current was 2.20 A m^{-1} flowing in the westward direction at 2054 UT. The current is quite clearly at its largest toward the end of the second expansion phase and during the recovery phase.

Following the first two Pi 2 pulsations, at 1936 and 2006 UT, the current reverses direction from westward to eastward. In both cases, however, the resultant maximum current was small, 200 mA m^{-1} after the first event and 75 mA m^{-1} after the second. The third event resulted in an enhancement of the westward current to 1.05 A m^{-1}. Another reversal in current direction followed the Pi 2 pulsation at 2042 UT, with the current peaking at 320 mA m^{-1}. This reversal coincided with both a reversal in the northward component of the electric field and a peak in Σ_H of 70.5 S, the highest value outside of the recovery phase. The Pi 2 pulsation at 2051 UT was followed by the peak current measured during the interval, 2.20 A m^{-1} at 2054 UT. A small enhancement in the current followed the Pi 2 at 2100 UT but not the final one at 2118 UT. All of the reversals in current direction or enhancements in current were related to similar reversals or enhancements in the north-south electric field.

There were a number of other peaks in the current (Figure 6), particularly following the final Pi 2 pulsation. Most of these were due to the electric field variation rather than the conductance, although the highest current during the recovery phase, 2.18 A m^{-1}, was related to the largest Σ_H in the complete interval. The significance of choosing peaks in current close to the Pi 2 pulsations is that these times relate to changes in the tail associated with substorm expansion phases. The peak currents are much larger than the AMIE estimates in the premidnight sector from substorm activity later in the SUNDIAL interval [*Lu et al.*, this issue]. The largest current density estimated in this later interval was of order 625 mA m^{-1} at the time of the second peak in the *AE* index during the expansion phase [*Lu et al.*, this issue]. Thus it seems in both cases the current was at its largest in the late expansion phase or early recovery phase in the premidnight sector.

We do not attempt to relate directly the current measured at EISCAT with the ground magnetic perturbations. One major problem with such a study is the limited area over which the radar measurements were made compared with the relatively large area over which the magnetometer averages. Furthermore, without any *E* region measurements of ion velocity, it is not possible to estimate the effect of neutral winds on the currents [*Kirkwood et al.*, 1988]. We note, however, that the zonal current was at its largest between 2042 and 2100 UT. The north-south component of the magnetic field (Figure 2) at the nearest staion to Tromsø, MAS (Figure 1), also reached a minimum in that time interval.

Kamide and Vickrey [1983] divided the nightside electrojets into three separate regions. The eastward electrojet was characterised as being dominated by a northward electric field. The westward electrojet was split into two local time sectors: the initial one in the midnight and early morning sector where the conductivity dominated a weak southward electric field, and a later one following 0300 LT where the southward electric field became dominant. Figure 5 demonstrates that the electric field following the pulsation at 2018 UT was southward and, although highly variable, was on average between 25 and 50 mV m^{-1}. The westward current was strongest only following the pulsation at 2042 UT. Thus the initial part of the westward electrojet was dominated by a southward electric field, and only after 2042 UT was the conductivity dominant. This differs from the picture suggested by *Kamide and Vickrey* [1983] and suggests that yet further spatial structure exists in the currents during these initial substorm phases.

5. Conclusions

In summary, simultaneous measurements of electric field and height-integrated Hall and Pedersen conductivities at a time resolution of 1 min and during an interval of substorm activity have been presented. The measurements were made in the premidnight sector and in the region of the eastward electrojet and substorm associated westward electrojet. Growth phase conductances were typical only of diffuse aurora while the current remained weakly westward. Peak values in Σ_H and Σ_P did not occur until well into the expansion phase or early in the recovery phase of the substorm. The ratio of the two conductances also changed during the interval, from less than 1 during the growth phase, to of order 1 during the early expansion phase to greater than 2 during the late expansion phase and recovery phase. Thus the average energy of the particles which caused the enhanced conductances increased during the substorm from less than 1 to ~ 10 keV. It is unclear if this is due to a significant temporal change in the acceleration process in the tail during the substorm cycle or to a spatial variation as the radar moves toward midnight.

Peak values of Σ_H and Σ_P were 76.5 and 40 S, respectively, during the recovery phase in the case of Σ_H and an earlier expansion phase in the case of Σ_P. The peak Σ_P is similar to those reported by *Kirkwood et al.* [1988] and *Aikio and Kaila* [1996], 48 and 40 S, respectively. The peak Σ_H is, however, much smaller than those reported by these authors, 120 and 214 S. The peak value in Σ_H also lead to a peak in the east-west current of 2.18 A m^{-1}, which was coincident with a minimum *X* perturbation at MAS. The east-west current either reversed or was enhanced following the first 6 of the 7 Pi 2 pulsations used to identify substorm expansion phases and intensifications. These reversals or enhancements in magnitude were a result of the electric field, irrespective of direction of current. These observations differ somewhat from those of *Kamide and Vickrey* [1983] who had suggested that the westward electrojet in this local time sector would be conductivity dominant. The work demonstrates that localised currents can often be larger than the average values, but, with the correct conductivity model, magnetic field perturbations can be inverted to get correct currents in the ionosphere. Further measurements at high time resolution of Σ_H and Σ_P, together with large spatial scales measurements of the electric field and auroral activity are necessary to investigate the spatial extent of the large values of conductance.

Acknowledgments. We would like to thank the members of the UK campaign team for running the EISCAT radar during this interval.

EISCAT is supported by the Suomen Akatemia (Finland), the Centre National de la Recherche Scientifique (France), the Max-Planck-Gesellschaft (Germany), the Norges Almenvitkenskapelige Forskingsråd (Norway), the Naturveterskapliga Forskningsrådet (Sweden), and the Particle Physics and Astronomy Research Council (United Kingdom). We would also like to thank David Orr for provision of SAMNET data, Hermann Lühr for provision of IMAGE data, and Geoff Reeves for provision of Los Alamos National Laboratory particle data.

The Editor thanks A. Brekke and another referee for their assistance in evaluating this paper.

References

Aikio, A.T., and K.U. Kaila, A substorm observed by EISCAT and other ground-based instruments - Evidence for near Earth substorm initiation, *J. Atmos. Terr. Phys., 58,* 5 - 21, 1996.

Baumjohann, W., R.J. Pellinen, H.J. Opgenoorth, and E. Nielsen, Joint two-dimensional observations of ground magnetic and ionosphere electric fields associated with local auroral break-ups, *Planet. Space. Sci., 29,* 431 - 447, 1981.

Belian, R.D., D.N. Baker, E.W. Hones, P.R. Higbie, S.J. Bame, and J.R. Ashbridge, Timing of energetic proton enhancements relative to magnetospheric substorm activity and its implication for substorm theories, *J. Geophys. Res., 86,* 1415 - 1421, 1981.

Brekke, A., J.R. Doupnik, and P.M. Banks, Incoherent scatter measurements of E region conductivities and currents in the auroral zone, *J. Geophys. Res., 79,* 3773, - 3790, 1974.

Brekke, A., C. Hall, and T.L. Hansen, Auroral ionospheric conductances during disturbed conditions, *Ann. Geophys., 7,* 269 - 280, 1989.

Davies, J.A., M. Lester, B. Jenkins, and R.J. Moffett, Dayside ion frictional heating: EISCAT observations and comparison with model results, *J. Atmos. Terr. Phys., 57,* 775 - 793, 1995.

Emery, B.A., et al., Electric potential patterns deduced for the SUNDIAL period of September 23-26, 1986, *Ann. Geophys., 8,* 399 - 408, 1990.

Farrugia, C.J., M.P. Freeman, L.F. Burlaga, R.P. Lepping, and K. Takahashi, The Earth's magnetosphere under continued forcing: Substorm activity during the passage of an interplanetary magnetic field, *J. Geophys. Res., 98,* 7657 - 7671, 1993.

Fuller-Rowell, T.J., and D.S. Evans, Height integrated Pedersen and Hall conductivity patterns inferred from the TIROS-NOAA satellite data, *J. Geophys. Res., 92,* 7606 - 7618, 1987.

Hedin, A.E., MSIS-86 thermospheric model, *J. Geophys. Res., 92,* 4649 - 4662, 1987.

Kamide, Y., and J.F. Vickrey, Relative contribution of ionospheric conductivity and electric field to the auroral electrojets, *J. Geophys. Res., 88,* 7989 - 7996, 1983.

Kirkwood, S., H. Opgenoorth, and J.S. Murphree, Ionospheric conductivities, electric fields and currents associated with auroral substorms measured by the EISCAT radar, *Planet. Space Sci., 36,* 1359 - 1380, 1988.

Knipp, D.J., A.D. Richmond, G. Crowley, O. de la Beaujardière, E. Friis-Christensen, D.S. Evans, J.C. Foster, I.W. McCrea, F.J. Rich, and J.A. Waldock, Electrodynamics patterns for September 19, 1984, *J. Geophys. Res., 94,* 16913 - 16923, 1989.

Lanchester B.S., K.U. Kaila, and I.W. McCrea, Relationship between large horizontal electric fields and auroral arc elements, *J. Geophys. Res., 101,* 5075 - 5084, 1996.

Lanzerotti, L.J., C.G. Maclennan, and M.F. Robbins, Proton drift echoes in the magnetosphere, *J. Geophys. Res., 76,* 259 - 263, 1971.

Lester, M., O. de la Beaujardiere, J.C. Foster, M.P. Freeman, H. Lühr, J.M. Ruohoniemi, and W. Swider, The response of the large scale ionospheric convection pattern to changes in the IMF and substorms: Results from the SUNDIAL 1987 campaign, *Ann. Geophys., 11,* 5567 - 571, 1993.

Lu, G., et al., High-latitude ionospheric electrodynamics as determined by the AMIE technique for the conjunctive SUNDIAL/ATLAS-1/GEM period of March 28-29, 1992, *J. Geophys. Res.,* this Issue.

Lühr, H., The IMAGE Magnetometer network, *STEP Int. Newsl. 4*(10), 4 - 6, 1994.

Lühr, H., S. Thurey, and N. Klocker, The EISCAT magnetometer cross. Operational aspects - First results, *Geophys. Surv., 6,* 305 - 315, 1984.

Lui, A.T.Y., A synthesis of magnetospheric substorms, *J. Geophys. Res., 96,* 1849 - 1856, 1991.

McCrea, I.W., M. Lester, T.R. Robinson, N.M. Wade, and T.B. Jones, On the identification and occurrence of ion frictional heating events in the high-latitude ionosphere, *J. Atmos. Terr. Phys., 53,* 587 - 597, 1991.

McPherron, R.L., C.T. Russell, and M.P. Aubry, Satellite studies of magnetospheric substorms on August 15, 1968, 9, Phenomenological model for substorms, *J. Geophys. Res., 78,* 3131 - 3149, 1973.

Mishin, V.M., S.B. Lunyushkin, D. S. Shiripov, and W. Baumjohann, A new method for generating instantaneous ionospheric conductivity models using ground-based magnetic data, *Planet. Space Sci., 34,* 713, 1986.

Opgenoorth, H.J., R.J. Pellinen, W. Baumjohann, E. Nielsen, G. Marklund, and L. Eliasson, Three-dimensional current flow and particle precipitation in a westward travelling surge (observed during the Barium-GEOS rocket experiment), *J. Geophys. Res., 88,* 3138 - 3152, 1983.

Reeves, G.D., R.D. Belian, and T.A. Fritz, Numerical tracing of energetic particle drifts in a model magnetosphere, *J. Geophys. Res., 96,* 13997 - 14008, 1991.

Richmond, A.D., and Y. Kamide, Mapping electrodynamic features of the high-latitude ionosphere from localised observations: Technique, *J. Geophys. Res., 93,* 5741 - 5759, 1988.

Robinson, R.M., R.R. Vondrak, K. Miller, T. Dabbs, and D. Hardy, On calculating ionospheric conductances from the flux and energy of precipitating particles, J. *Geophys. Res., 92,* 2565 - 2569, 1987.

Rostoker, G., S.-I. Akasofu, J. Foster, R.A. Greenwald, Y. Kamide, K. Kawasaki, A.T.Y. Lui, R.L. McPherron, and C.T. Russell, Magnetospheric substorms - definition and signatures, *J. Geophys. Res., 85,* 1663, 1980.

Spiro, R.W., P.H. Reiff, and L.J. Maher Jr., Precipitating electron energy flux and auroral zone conductances - an empirical model, *J. Geophys. Res., 87,* 8215 - 8227, 1982.

Szuszczewicz, E.P., et al., *F* region climatology during the SUNDIAL/ATLAS-1 campaign of March 1992: Prevailing conditions and model-measurement comparisons, *J. Geophys. Res.,* this issue.

Torr, M.R., The scientific objectives of the ATLAS-1 shuttle mission, *Geophys. Res. Letts., 20,* 487 - 490, 1993.

Williams, P.J.S., T.S. Virdi, S.W.H. Cowley, and M. Lester, Short-lived bursts of plasma velocity in the auroral zone, I, Observational evidence from radar measurements, *J. Atmos. Terr. Phys., 52,* 421 - 430, 1990.

Williams, P.J.S., R.V. Lewis, T.S. Virdi, M. Lester, and E. Nielsen, Plasma flow bursts in the auroral electrojets, *Ann. Geophys., 10,* 835-848, 1992.

Yeoman, T.K., D.K. Milling, and D. Orr, Pi2 polarisation patterns on the UK Sub-Auroral Magnetometer Network (SAMNET), *Planet. Space Sci., 38,* 589 - 602, 1990.

Yeoman, T.K., M.P. Freeman, G.D. Reeves, M. Lester, and D. Orr, A comparison of mid-latitude Pi2 pulsations and geostationary orbit particle injections as substorm indicators, *J. Geophys. Res., 99,* 4085 - 4093, 1994.

J. A. Davies and M. Lester, Radio and Space Plasma Physics Group, Department of Physics and Astronomy, University of Leicester, Leicester LE1 7RH, England.

T. S. Virdi, Department of Physics, University College Wales, Aberystwyth, Dyfed, SY23 3BZ, Wales.

(Received September 14, 1995; revised March 1, 1996; accepted March 25, 1996.)